Effect of pressure on the band gap and the local FeO_6 environment in $BiFeO_3$

Susana Gómez-Salces,[1] Fernando Aguado,[1] Fernando Rodríguez,[1,*] Rafael Valiente,[2] Jesús González,[1] Raphael Haumont,[3] and Jens Kreisel[4]

[1]*MALTA-Consolider Team, DCITIMAC, Universidad de Cantabria, Santander, Spain*

[2]*MALTA-Consolider Team, Departamento de Física Aplicada, Universidad de Cantabria, Santander, Spain*

[3]*ICMMO, Université Paris XI, Orsay, France*

[4]*Laboratoire des Matériaux et du Génie Physique, Minatec, CNRS, Grenoble Institute of Technology, Grenoble, France*

(Received 12 January 2012; revised manuscript received 21 March 2012; published 16 April 2012)

$BiFeO_3$ exhibits a complex phase-transition sequence under pressure associated with changes in octahedron tilts and displacements of Bi^{3+} and Fe^{3+} cations. Here, we investigate the local structure of Fe^{3+} as a function of pressure through absorption crystal-field spectroscopy in the 0–18 GPa range. We focus on the influence of phase transitions on the Fe^{3+} off-center displacement through the energy (E) and oscillator strength (f_{d-d}) of the $^4T_1$ and $^4T_2$ Fe^{3+} ($3d^5$) bands observed below the band gap ($E_{gap} = 2.49$ eV) at 1.39 and 1.92 eV, respectively, at ambient conditions. Pressure induces linear redshift of both $^4T_1$ and $^4T_2$ bands, consistent with the compression of the FeO_6 octahedron under pressure. On the other hand, the transition oscillator strength ($f_{d-d} = 3 \times 10^{-5}$), enabled by both the exchange mechanism and the off-center Fe^{3+} distortion, slightly increases with pressure. The absence of notable anomalies in the variation of $E(P)$ and $f_{d-d}(P)$ through the phase sequence from the ferroelectric rhombohedral $R3c$ phase to the nonpolar orthorhombic $Pnma$ phase suggests a persisting off-center position of the Fe^{3+}. While this local polarity is correlated and expected in the ferroelectric $R3c$ phase, its presence in the high-pressure nonpolar $Pnma$ phase indicates the presence of local polar instabilities.

DOI: 10.1103/PhysRevB.85.144109 PACS number(s): 81.40.Vw, 77.80.B−, 71.70.Ch, 78.40.Ha

I. INTRODUCTION

In the past much progress in understanding ferroic properties, such as ferroelasticity or ferroelectricity, and their related phase transitions has been achieved through temperature- or chemical composition-dependent investigations. The use of pressure for the investigation of ferroic ABO_3 perovskites has been much less common and was mostly limited to pressures below 10 GPa.[1–3] The experimental difficulty has now been overcome for a number of years and our understanding of phase transitions and coupling mechanism in functional perovskites has been recently significantly improved, thanks to an increasing number of investigated perovskites,[4] namely ferroelectrics[5–8] and ferroelastics.[9–13] The pressure dependences in diamond anvil cells (DAC) can now be analyzed with a similar accuracy as the more traditional temperature dependences.

Nevertheless, a precise structural analysis in terms of a structural refinement is more difficult in high-pressure DAC experiments due to the absorbing sample environment, which often inhibits the access to reliable intensities and thus the determination of precise atomic positions. As a consequence, it remains challenging to follow quantitatively two of the main structural distortions in the perovskite structure[14–16] via high-pressure diffraction experiments: (i) the tilt of the BO_6 octahedra and (ii) polar cation displacements inside the BO_6 or AO_{12} polyhedra. The distortion in tilted perovskites in the high-pressure set-up is best followed by the intensity of weak but observable cell-doubling superstructure reflections (see $LaAlO_3$,[11,12] $SrTiO_3$,[10] or $CaTiO_3$[9]). In the case of ferroelectrics, the polar distortion is usually followed through unit cell distortion such as the c/a tetragonality in $PbTiO_3$.[6]

However, the situation is notoriously more complex when both tilt and polar distortions occur within the same phase, as might occur for some perovskites at very high-pressure[5,6,17] or namely in multiferroic materials. In such materials the tilts can still be, at least qualitatively, followed via the intensity of the superstructure reflections provided that there is no other cell doubling phenomena such as antiferroelectricity or chemical order. On the other hand, the cell distortion as measured by the peak splitting is now a result of both tilts and cation displacement, which inhibits the distinction between a ferroelectric and nonferroelectric phase. Also, nonferroelectric phases may in certain cases present disordered structures of local electric dipoles associated with off-center cation displacements (paraelectric or electric-dipole glasslike structures), which are at best difficult to detect from diffraction measurements. In such a case, the use of sensitive local probes is essential to unravel such local off-center polar displacements. Examples of order-disorder and displacive phase transitions associated with off-center displacements have been reported by x-ray absorption spectroscopy (XAS) and x-ray diffuse scattering in perovskite oxides like $KNbO_3$ (Refs. 18 and 19), $BaTiO_3$, (Refs. 19 and 20), or $SrTiO_3$ (Refs. 21 and 22).

Our study focuses on $BiFeO_3$, which can be considered as a model multiferroic material with strong tilt and polar distortions at room temperature (RT).[23] Despite a number of high-pressure investigations in $BiFeO_3$,[24–35] the polar character of the low pressure ($P < 10$ GPa) is still not clear, and, consequently, the competition and coupling between tilts and polarity is not clear either.

The aim of this paper is to investigate the polar distortions around Fe^{3+} in $BiFeO_3$ as a function of pressure along the different high-pressure phases by using optical absorption and Raman spectroscopy as probes for Fe^{3+} local structure and pressure-induced phase-transition sequence.

II. EXPERIMENTAL

Single crystals of $BiFeO_3$ were grown by the flux method, as described elsewhere.[36] The rhombohedric $R3c$ crystal

structure was checked by x-ray diffraction (XRD) and Raman spectroscopy and the optical quality by means of a polarizing microscope. The microcrystals used in pressure experiments ($90 \times 70 \times 30$ μm^3) were extracted by cleavage from a $BiFeO_3$ single crystal. The Raman spectra were taken with a Horiba T64000 triple spectrometer using the 514.5 nm and 647 nm lines of a Coherent Innova Spectrum 70C Ar^+-Kr^+ laser and a nitrogen-cooled CCD (Jobin-Yvon *Symphony*) with a confocal microscope for detection. For measuring the low frequency modes we used the triple monochromator in the subtractive configuration. The experimental set-up used for RT optical absorption measurements for use with DAC has been described elsewhere.[37,38] The detection setup was equipped with a photomultiplier (Hamamatsu R928S) and an InGaAs detector for measurements in the VIS and NIR range, respectively. The 220-Hz modulated light from a tungsten lamp was dispersed with a 0.5-m single monochromator (Chromex 500IS/SM), and the detected signal was analyzed with a lock-in amplifier (Stanford Research SR830). Polarization measurements at ambient condition in oriented microcrystal plates were taken in the same absorption setup by inserting a Glan-Taylor polarizer prism between the sample and the microscope objective. High pressure measurements were carried out in gasketed membrane DAC with both paraffin oil and methanol-ethanol-water (16 : 3 : 1) as transmitting media for Raman and optical absorption experiments. Pressure was calibrated from the ruby R-line luminescence shift.

III. PRELIMINARY REMARKS

The idea for using optical absorption spectroscopy in this study is based on the high sensitivity of crystal-field electronic transitions of Fe^{3+} ($3d^5$) to slight distortions of coordination octahedron FeO_6.[39–41] Both the transition energy and oscillator strength strongly depend on the Fe-O bond length, site symmetry and Fe–O–Fe exchange interaction. In particular, the first two crystal-field transitions, $^6A_1 \rightarrow {}^4T_1$ and $^4T_2$, are the only ones detected below the gap absorption threshold in $BiFeO_3$ and $(R)FeO_3$ (R: rare earth).[42–45] Their energy decreases proportional to the increase of the crystal-field splitting, Δ, whereas their oscillator strength, f_{d-d}, which is for both parity and spin forbidden in isolated centrosymmetric FeO_6 centers ($f_{d-d} \approx 10^{-7}$), can vary several orders of magnitude depending on the activation mechanism.[41,46] Thermal activation by odd parity vibrations, pairwise mechanism between exchange coupled Fe^{3+} pairs, noncentrosymmetric static distortions, or a combination of these can activate the transition enabling its detection by optical absorption.[39–41] Previous optical absorption experiments as a function of pressure in $BiFeO_3$[27–30,44] were focused on the variation of the band gap energy at the high-spin to low-spin transition around 50 GPa. The authors conclude that the band gap closure ($E_{gap} = 0$) correlates with the sample metallization taking place at the same spin crossover pressure. However the low-energy Fe^{3+} bands were not observed probably due to their relatively low intensity and the fact that they are masked by the tail of band gap absorption above 18 GPa. A review of *d*-*d* transitions in orthoferrites and ferric borates as a function of pressure can be found in Ref. 44, where the emphasis was paid on the pressure dependence of the $^4T_1$ and $^4T_2$ transition energy, while their intensity (i.e., oscillator strength f_{d-d}) dependence remained unexplored.

In this paper, we investigate the pressure dependence of both the energy and oscillator strength of these Fe^{3+} bands in $BiFeO_3$ in the 0–18 GPa range, aiming to investigate the local structure around Fe^{3+} through the reported phase-transition sequence.[34] In particular, we are interested in elucidating whether the nonpolar orthorhombic *Pnma* phase above 10 GPa is truly nonpolar or if it keeps a Fe off-center distortion on a local level. This information is at best difficult to extract from XRD[34] but important to understand the structural competitions in $BiFeO_3$.

First, we present the Raman data as a structural characterization technique in pressure experiments. Second, the absorption measurements as a function of pressure is presented, and finally an analysis of data regarding the pressure effect on the local structure of Fe^{3+} will be discussed.

IV. RESULTS AND DISCUSSION

A. Pressure-induced phase transitions through Raman spectroscopy

Figure 1 shows the variation of the cell volume of $BiFeO_3$ in the 0–14 GPa range obtained from XRD.[26,34] Despite several pressure-induced phase transitions,[34] $V(P)$ exhibits a close to continuous behavior with only slight anomalies in this pressure range, which we approximate here by a Murnaghan equation of state with $K_0 = 122$ GPa (Fig. 1). In this figure the phase-transition sequence and associated critical pressures, derived from XRD, are indicated by vertical lines, defining the pressure range of stability of each phase. The Raman spectrum of $BiFeO_3$ and its variation with pressure in the 0–10 GPa range are shown in Fig. 2. The spectra were taken together with the optical absorption spectra for crystal phase characterization. The Raman spectrum at ambient conditions

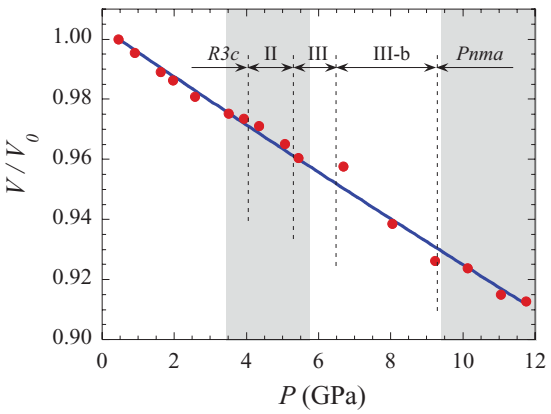

FIG. 1. (Color online) Pressure evolution of the pseudocubic cell volume in $BiFeO_3$ using paraffin as pressure transmitting medium. $V/V_0(P)$ data are collected elsewhere (Ref. 26). The stability domains of the various phases represented as colored stripes are given for hydrostatic conditions, while the phase sequence observed in nonhydrostatic conditions is indicated by the dashed lines in the volume plot (Ref. 34). The line corresponds to the fitting of experimental data to a Murnaghan equation of state with $K_0 = 122$ GPa. Given the linear dependence of $V(P)$, we fit the equation using $K' = 0$.

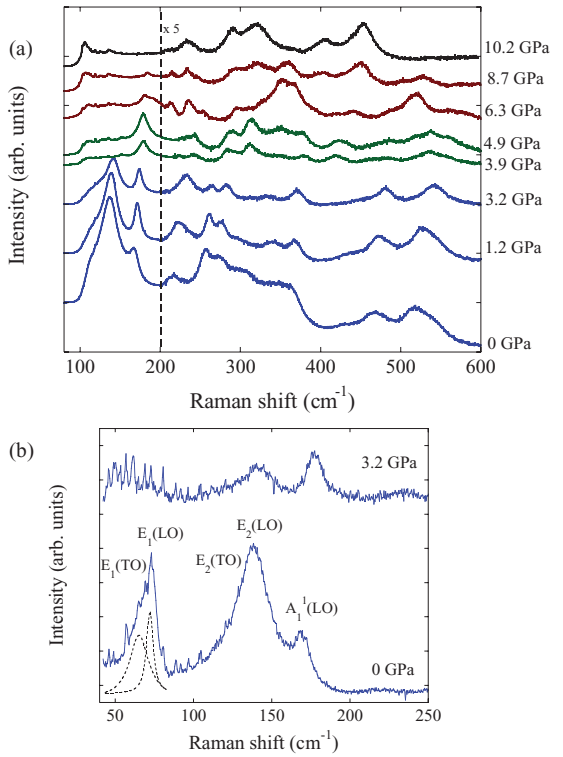

FIG. 2. (Color online) Single crystal Raman spectrum of $BiFeO_3$ as a function of pressure: (a) Raman modes in the 100–600 cm^{-1} range; (b) low frequency modes associated with the Bi–O bonds. The dotted lines represent the fit to two Lorentzians corresponding to the E_1(TO) and E_1(LO) phonons at 65 and 72 cm^{-1}, respectively. The narrow-line features appearing below 120 cm^{-1} at 0 and 3.2 GPa correspond to rotational modes of the atmospheric N_2 molecule. Vibrational mode assignment and peak frequencies are collected in Table I.

TABLE I. Symmetry, frequency (ν_0), pressure derivative ($d\nu_i/dP$), Grüneisen parameter (γ) of the Raman active modes of $BiFeO_3$ single crystal measured at ambient temperature in the low-pressure $R3c$ phase ($P < 3.4$ GPa).

Mode symmetry	ν_0 (cm^{-1})	$\frac{d\nu_i}{dP}$ ($cm^{-1}GPa^{-1}$)	γ
E_1(TO)	65	1.46	2.74
E_1(LO)	72	2.74	4.64
E_2(TO)	137	1.75	1.57
E_2(LO)	139	1.45	1.29
$A_1{}^1$(LO)	167	2.06	1.50
$A_2{}^1$(LO)	216	4.29	2.42
E_3(TO)	256	1.78	0.86
E_4(TO)	274	3.71	1.65
E_5(TO)	304	6.04	2.42
E_6(TO)	349	− 3.06	− 1.07
E_7(TO)	366	1.30	0.43
E_8(TO)	429	9.17	2.60
$A_3{}^1$(TO)	467	3.73	0.97
E_9(TO)	524	6.34	1.48
$A_4{}^1$(TO)	541	5.35	1.21

Grüneisen parameter: $\gamma = \frac{1}{\nu_0} K_0 \frac{d\nu_i}{dP}$, where $K_0 = 122$ GPa.

consists of 13 peaks, which correspond to $4A_1 + 9E$ modes of the rhombohedral $R3c$ space group and is consistent with XRD and previous Raman data.[34,43,47] Their assignment, Raman frequency, and the associated Grüneisen parameter are given in Table I. Its evolution with pressure shows changes of both the frequency mode shift and the number of Raman modes, which reflect the presence of at least three different structural phases. According to XRD data (Fig. 1), these are in order of increasing pressure: $R3c$; three intermediate orthorhombic phases, denoted by $O1$, $O2$, and $O3$ (or Phases II, III, and III-b); and the orthorhombic $Pnma$ high pressure phase.[26,34] The associated phase-transition pressures have been determined by Raman spectroscopy through the abrupt changes in the peak structure and the slopes of the $\nu(P)$ curve (Fig. 3). Three phase transitions observed upon increasing pressure are $R3c \rightarrow O1$ at 3.4 GPa; $O1 \rightarrow O2,O3$ at 5.5 GPa; and $O2,O3 \rightarrow Pnma$ at 9.5 GPa. In Fig. 2(b) we observe how the low frequency E_1(LO-TO) modes vanish with pressure at the phase transition $R3c \rightarrow O1$. This Raman peak has been associated to Bi-O vibrations. Recent infrared and Raman measurements have shown that this mode is the soft mode of the $BiFeO_3$ ferroelectric transition.[48–50] The precise determination of the phase-transition pressures has been done with the E_2(TO), $A_1{}^1$(LO), and E_6(TO), E_8(TO) modes, since they provide marked frequency shift changes at the phase-transition pressure, as illustrated in Fig. 3. The variation of the intense E_2(TO) peak at 137 cm^{-1} is noteworthy. Its intensity reduces with pressure in the rhombohedral phase and completely disappears in the orthorhombic phases at 3.4 GPa [Fig. 2(b)]. It must be noted that the Raman spectroscopy is a well suited technique to detect the $O1 \rightarrow O2,O3$ transition but is more difficult to discriminate between $O2$ and $O3$ phases. However, these phases were clearly identified by XRD.[34]

B. Optical absorption as a function of pressure

Figure 4 shows the polarized optical absorption spectrum of $BiFeO_3$ at ambient conditions with the electric field of the light pointing nearly parallel to the ferroelectric direction (π) and perpendicular to it (σ). In agreement with literature on ferrite compounds,[42,44] the spectrum consists of two weak bands at 1.39 eV and 1.92 eV and an intense absorption edge above 2.2 eV, which are assigned to $3d^5$-intraconfigurational $^6A_1 \rightarrow {}^4T_1$ and $^4T_2$ crystal-field transitions (Fig. 5) and band-gap transition involving mainly 6p-Bi levels and $O^{2-} \rightarrow Fe^{3+}$ charge-transfer states in the conduction band, respectively.[45] Note that the first $^4T_1$ absorption band exhibits a remarkable anisotropy when the light-polarization points along ferroelectric direction clearly pointing out the noncentrosymmetric Fe^{3+} site in $BiFeO_3$ and contrasts with the absence of polarization behavior of Fe^{3+} optical absorption in orthoferrites where iron has a nearly regular octahedral coordination FeO_6. Furthermore, the absorption coefficient of the two d-d Fe^{3+} bands in $BiFeO_3$ are approximately three times higher than the corresponding transitions in orthoferrites $(R)FeO_3$ (R = Ho, Pr, Gd; Y, Er, Lu)[42,44] or ferric borate $FeBO_3$ (Refs. 44 and 51). The transition oscillator strength (f_{d-d}) can be derived

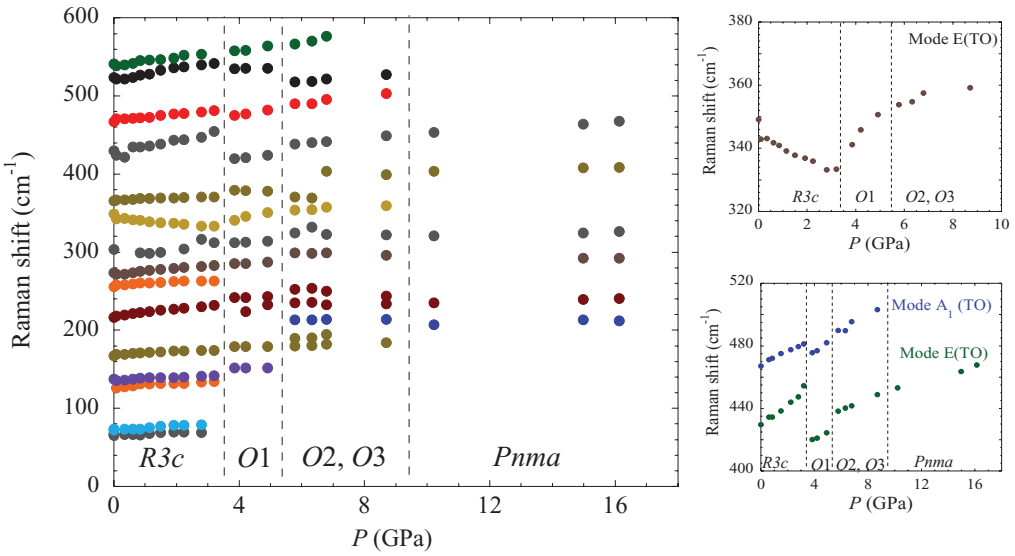

FIG. 3. (Color online) Pressure dependence of the Raman mode frequency in the 0–18 GPa range. Vertical dashed lines indicate the structural phase-transition pressures: $R3c \rightarrow O1$; $O1 \rightarrow O2,O3$; and $O3 \rightarrow Pnma$ (see text). Different variations of the frequency with pressure for selected Raman modes are shown right side.

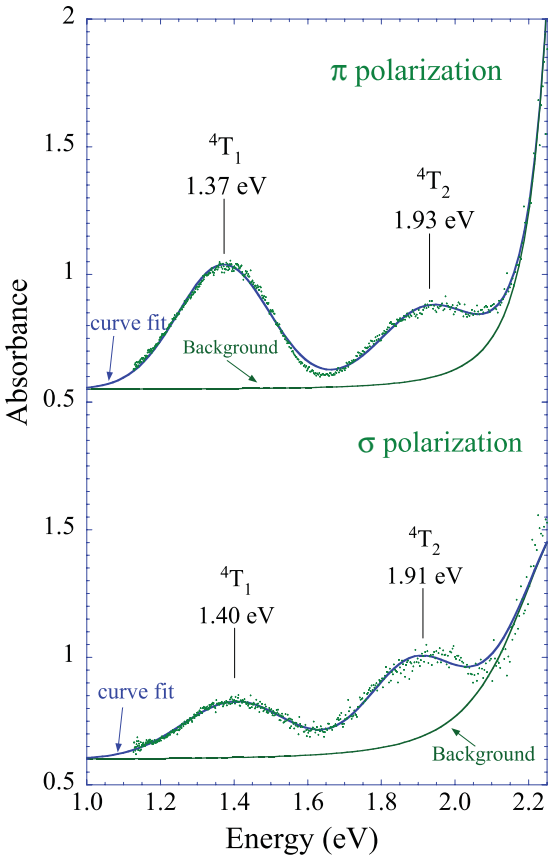

FIG. 4. (Color online) Single-crystal polarized optical-absorption spectra of $BiFeO_3$ at ambient conditions. π and σ denote electric field of light nearly along the ferroelectric direction and perpendicular to it, respectively. Sample thickness: 30 μm. The blue (solid wavy) line corresponds to the fit absorption spectrum to the sum of two Gaussians for the $^4T_1$ and $^4T_2$ crystal-field bands of Fe^{3+} and a Lorentzian-type background associated with the band gap absorption.

from the integrated absorption through the equation[52]

$$f_{d-d} = 8.20 \times 10^{16} \frac{n_r}{(n_r^2+2)^2} \frac{\int_{\text{band}} \alpha dE}{N} \qquad (1)$$

where $n_r = 2.7$ is the $BiFeO_3$ refractive index,[53] $N = 1.61 \times 10^{22}$ cm^{-3}, the Fe^{3+} concentration, and α and E the absorption coefficient (in cm^{-1}) and photon energy (in eV) of the $^4T_1$ (or $^4T_2$) band, respectively. The average oscillator strength for $^4T_1$ at ambient conditions derived from the polarized absorption spectra is $f_{d-d} = 3 \times 10^{-5}$. It must be pointed out that although this value is small in comparison to typical electric-dipole $s \rightarrow p$ allowed transitions or $O^{2-} \rightarrow Fe^{3+}$ charge transfer transitions ($f \approx 0.1$), it is however rather high for $^6A_{1g} \rightarrow {}^4T_{1g}$ (or $^4T_{2g}$) since these transitions are spin and parity forbidden in centrosymmetric systems, thus having oscillator strengths of about $f_{d-d} \approx 10^{-7}$ (Ref. 46). As we will discuss later, the exchange mechanism between Fe^{3+} pairs in concentrated systems and noncentrosymmetric crystal-field distortions around Fe^{3+} such as those attained in $BiFeO_3$ and Fe_2O_3 both relax the spin and parity forbiddingness, enhancing the transition oscillator strengths by two orders of magnitude with respect to isolated centrosymmetric FeO_6 systems.[39,41,46,54] The integrated band intensity and the transition energy for $^4T_1$ and $^4T_2$ have been both obtained by fitting the optical absorption spectra to the sum of two Gaussians and band-gap background absorption (Fig. 4). This procedure allows us to extract integrated intensity of each band, the transition oscillator strength through Eq. (1), the crystal-field transition energies, and the gap energy as a function of pressure. Figure 6 shows the pressure dependence of the absorption spectrum and corresponding fits. Three relevant features are observed: (i) both the $^4T_1$ and $^4T_2$ bands redshift with pressure, (ii) the absorption intensity associated with these transitions does not notably change with pressure

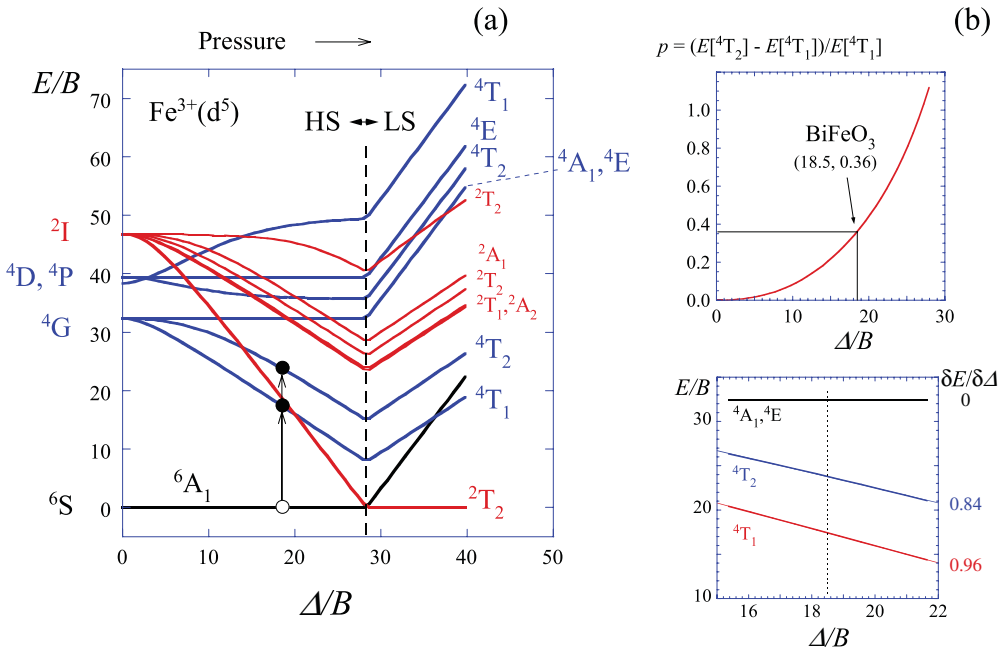

FIG. 5. (Color online) (a) Tanabe-Sugano diagram for d^5 ions calculated for $C/B = 4.5$. The state energy (E/B) for the ^{2}I, ^{4}D, ^{4}P, ^{4}G, and ^{6}S Fe^{3+}-ion multiplets is referred to the ground state ^{6}A$_1$ (high spin) or ^{2}T$_2$ (low spin) as a function of the crystal field strength (Δ/B). The points represent the ^{4}T$_1$ and ^{4}T$_2$ energies of Fe^{3+} in BiFeO$_3$ at ambient conditions. The effect of pressure is qualitatively represented on the top abscissa axis. (b) Modified Tanabe-Sugano diagrams for the first two crystal-field transitions of Fe^{3+} ($3d^5$). The parameter p defined as the ^{4}T$_1$ − ^{4}T$_2$ energy difference to the ^{4}T$_1$ energy is very sensitive to Δ/B for Racah parameter C/B ratio between 4 and 5. The ambient pressure parameter for BiFeO$_3$, $p = 0.36$, corresponds to $\Delta/B = 18.5$. The deduced crystal-field parameters are $\Delta = 1.5$ eV (12 100 cm^{-1}) and $B = 81$ meV (653 cm^{-1}). The slopes of $E(\Delta)$ for ^{4}T$_1$, ^{4}T$_2$ and ^{4}A$_1$, ^{4}E$_2$ are given on the right side in the figure.

in the explored 0–18 GPa range, and (iii) the absorption band gap threshold shifts to lower energies with pressure. The fits shown on the right side of Fig. 6 provide E_{gap}, $E(^4T_1)$, and $E(^4T_2)$, as well as $f_{d-d}(^4T_1)$ and $f_{d-d}(^4T_2)$. Their variation with pressure is represented in Figs. 7–9.

Concerning pressure-induced energy shifts, the different $E(P)$ behavior exhibited by the band gap and the crystal-field peaks is noteworthy. Although both shift to lower energy with pressure, $E_{gap}(P)$ varies differently in each phase, whereas $E(^4T_1)$ and $E(^4T_2)$ depends linearly on pressure in the explored pressure range, independently of the crystal structure. This fact points out how the band gap, as a crystal bulk property, depends on the crystal structure and thus is a well-suited probe for detecting phase transitions. In contrast to $E_{gap}(P)$, the Fe^{3+} crystal-field energy mainly depends on the FeO$_6$ local structure and therefore is more sensitive to changes of the Fe^{3+} coordination than to the crystal structure. Figure 7 illustrates the three different behaviors of $E_{gap}(P)$ in the 0–18 GPa range. We observe a clear change on the $E_{gap}(P)$ slope at the $R3c \rightarrow O1$ and $O3 \rightarrow Pnma$ phase-transition pressures at 3.4 and 9.5 GPa, respectively. Between these pressures, the dispersion of data in $E_{gap}(P)$ prevents us to detect the $O1 \rightarrow O2$ and $O2 \rightarrow O3$ phase transitions. However, their presence is known from a recent study by Raman spectroscopy and XRD, which reports transition pressures at 5 and 7 GPa, respectively.[34] A relevant aspect of $E_{gap}(P)$ is its sensitivity for detecting the two prominent crystal phase transitions $R3c \rightarrow O1$ and $O3 \rightarrow Pnma$. Furthermore, the abrupt jump of $\partial E_{gap}/\partial P$ at the phase transition allows us an accurate determination of the transition pressure using the optical band gap from absorption spectra.

It must be noted that optical absorption measurements in BiFeO$_3$ under pressure have been previously performed to investigate pressure-induced gap closure in connection with metallization process and spin transition phenomena at about 50 GPa.[27–30] However, such studies mainly focused on the strong variation of the band gap near the metallization pressure, but the phase-transition effects on the band gap at moderate pressures went unnoticed. In the present work, we perform precise absorption measurements on BiFeO$_3$ under pressure showing the adequacy of $E_{gap}(P)$ to unravel phase-transition pressure as well as the observation of Fe^{3+} crystal-field bands (uninvestigated in previous works[27–30]) for structural correlations at high pressure.

C. Local structure of Fe^{3+} in BiFeO$_3$

Unlike the energy gap, the ^{4}T$_1$ and ^{4}T$_2$ bands of Fe^{3+} show neither significant changes with pressure nor anomalies at phase-transition pressures. By contrast, the peak positions, which are strongly dependent on the Fe^{3+} local coordination, shift linearly with pressure at a pressure rate consistently with the crystal compression[55,56] (crystal-field theory[57]). The observation of two bands at 1.39 eV (^{4}T$_1$) and 1.92 eV (^{4}T$_2$) at ambient conditions is due to Fe^{3+} in octahedral coordination FeO$_6$ similarly to other absorption spectra in (R)FeO$_3$ (R: rare earth), FeBO$_3$, Y$_3$Fe$_5$O$_{12}$, and Fe$_2$O$_3$. Besides some Fe^{3+} compounds where the first three ^{6}A$_1 \rightarrow$ ^{4}T$_1$, ^{4}T$_2$, and ^{4}A$_1$, ^{4}E

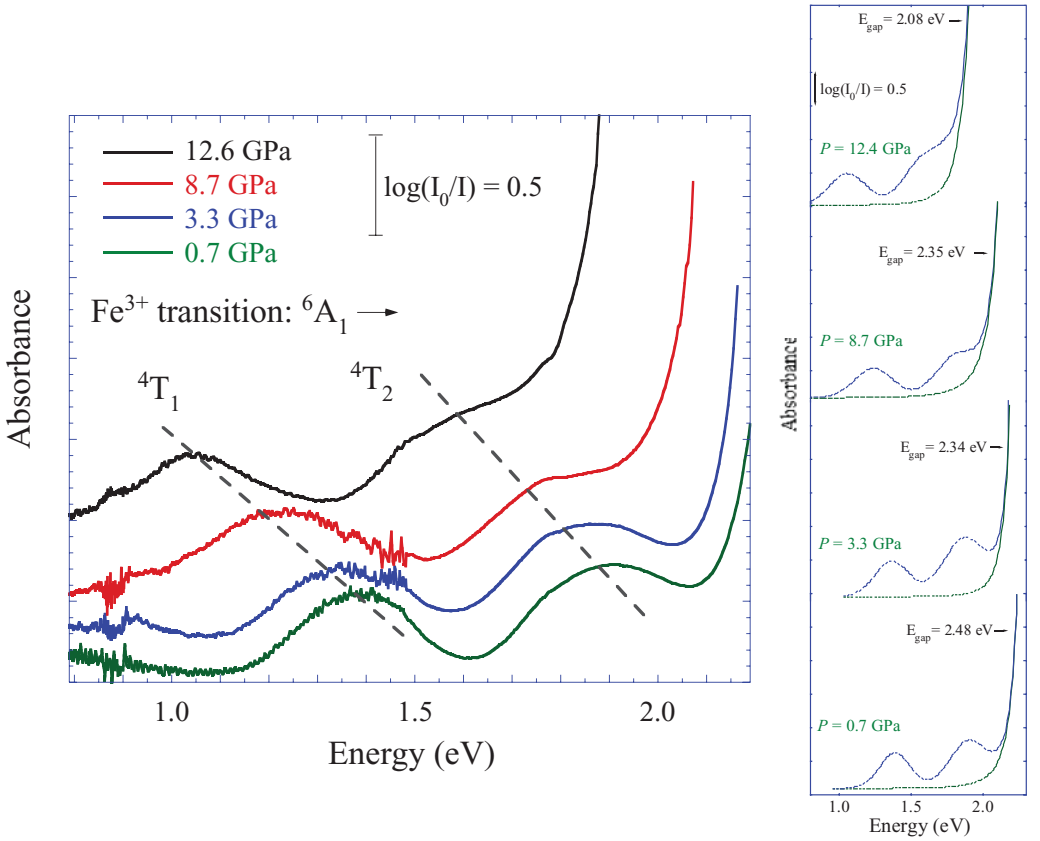

FIG. 6. (Color online) Variation of the room-temperature unpolarized optical absorption spectrum of $BiFeO_3$ with pressure. Note the pressure-induced redshift of both $^4T_1$ and $^4T_2$ crystal-field bands of Fe^{3+} and the band gap. Slashed lines are guide for the eye. The fit of each optical absorption spectrum to the sum of two Gaussians for $^4T_1$ and $^4T_2$ bands and a Lorentzian-type background associated with the band gap absorption is given on the right side. Crystal thickness: 30 μm.

crystal-field transitions are observed, only the first two can be detected in $BiFeO_3$ because the third $^4A_1$,^4E band is masked by the band gap. Nevertheless, the $^6A_1 \rightarrow {}^4A_1$,$^4E$ transition energy, unlike $^4T_1$ and $^4T_2$, does not depend, in first approximation, on the crystal-field strength Δ so that its energy can be easily estimated from the Tanabe-Sugano diagrams and similar compounds provided that we know the $^4T_1$ and $^4T_2$ energies (Fig. 5). In fact, $E(^4A_1,{}^4E)$ varies from 2.3 eV ($NdFeO_3$)[44] to 2.8 eV ($FeBO_3$)[51] passing through intermediate values like 2.6 eV ($Y_3Fe_5O_{12}$).[46] The absorption threshold in $BiFeO_3$ starting at 2.2 eV precludes any observation of this transition.

Besides some slight anomalies observed around 9 GPa, the overall $E(P)$ variation for $^4T_1$ and $^4T_2$ decreases linearly with pressure at a rate of -21 and -19 meV/GPa, respectively (Fig. 8). This pressure behavior is similar to that observed in $3d^5$ ions like Mn^{2+}, or Fe^{3+} for $^4T_1$ and $^4T_2$ in sixfold coordination under pressure.[44,55,56,58] Volume reduction increases the e-t_2 crystal-field splitting, Δ, leading to a redshift of the first two $^4T_1$ and $^4T_2$ bands according to the Tanabe-Sugano diagrams (Fig. 5). Although Δ and Racah (B and C) parameters are hard to derive from only $^4T_1$ and $^4T_2$, we have established a methodology for extracting such spectroscopic quantities through the parameter p defined as $p = \frac{E[^4T_2]-E[^4T_1]}{E[^4T_1]}$, from which the ratio Δ/B can be obtained independently of the particular choice of the C/B ratio between 4 and 5 (Fig. 5). The advantage of p for such an analysis

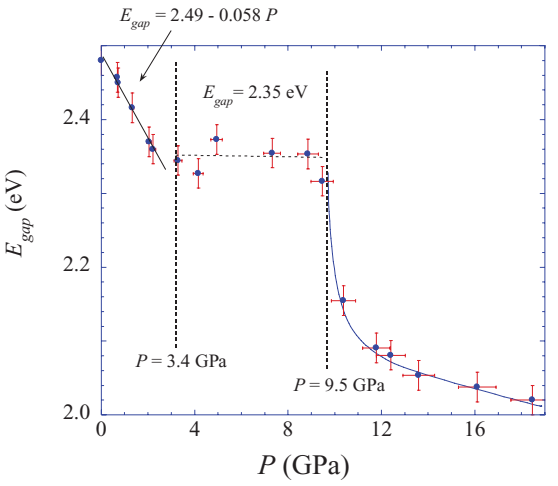

FIG. 7. (Color online) Variation of the energy gap, E_{gap}, of $BiFeO_3$ with pressure. E_{gap} was derived by fitting the optical absorption spectra to band-gap absorption. Note the three different regimes of $E_{gap}(P)$. The abrupt changes of $E_{gap}(P)$ slopes correspond to critical pressures associated with structural phase transition in $BiFeO_3$. A linear behavior at a rate of 58 meV/GPa is observed in the rhombohedral $R3c$ phase below 3.4 GPa; a nearly pressure-independent behavior with $E_{gap} = 2.35$ eV between 3.4 and 9.5 GPa; and abrupt redshift variation is detected above 9.6 GPa. The energy gap decreases by 0.5 eV from ambient pressure to 18 GPa.

is twofold: (i) p is a nondimensional parameter and does not explicitly depend on Δ or B but on Δ/B; and (ii) it strongly varies with Δ/B, as illustrated in Fig. 5(b). Its steep variation allows us a precise determination of Δ/B. From the experimental value $p = 0.36$, we obtain $\Delta/B = 18.5$ at $P = 0$ GPa, which corresponds to $\Delta = 1.50$ eV and $B = 81$ meV according to the E/B versus Δ/B Tanabe-Sugano diagram (Fig. 5) and the measured $^4T_1$ and $^4T_2$ energies at ambient conditions (Fig. 4). Interestingly, from these parameters we deduce that the $^4A_1$,^4E peak energy ($E = 10B + 5C$) should be 2.63 eV for $C/B = 4.5$. This estimate is in agreement with those energies measured for Fe^{3+} in oxides and supports method adequacy.

The pressure dependence of $^4T_1$ and $^4T_2$ indicates that Δ and B do vary with pressure, as $\partial\Delta/\partial P = 22$ meV/GPa and $\partial B/\partial P = -0.4$ meV/GPa. These values are similar to those measured in octahedral isoelectronic Mn^{2+} systems under pressure,[55,58] as well as in Cr^{3+} in oxides.[41,55] On the assumption of an R-dependence of the crystal-field splitting as $\mathbf{\Delta} = kR^{-n} = k'V^{-n'/3}$, with R and V being the Fe-O bond length and the crystal volume, respectively. Note that we allow for an eventual different scaling of $\Delta(R)$ and $\Delta(V)$ through the exponent n. We can derive n' from the measured pressure dependences using the bulk modulus derived from the equation of state in the 0–14 GPa range (Fig. 1). So the volume dependence of Δ is given by

$$n' = \left(\frac{3K_0}{\Delta}\right)\left(\frac{\partial\Delta}{\partial P}\right)_T. \quad (2)$$

Using $K_0 = 122$ GPa, $\Delta = 1.50$ eV, and $\partial\Delta/\partial P = 22$ meV/GPa, we obtain $n' = 5.4 \approx 5$. Although this exponent is slightly higher than the value $n = 5$ given in previous experimental and theoretical studies in transition metal oxides,[41,55] it means that the crystal and the local FeO_6 bulk moduli are approximately the same; i.e., the Fe–O bond length compresses similarly to the cell parameters.

The oscillator strength of the $^4T_1$ and $^4T_2$ Fe^{3+} bands derived from the integrated band intensity through Eq. (1) shows a linear behavior with pressure (Fig. 8). The slight linear increase of f_{d-d} with pressure is noteworthy as it suggests that Fe^{3+} occupies a noncentrosymmetric site in the explored pressure range even up to 18 GPa. According to this result, the off-center position, which is concomitant with the ferroelectric rhombohedral $R3c$ phase at ambient conditions, still persists in the nonpolar orthorhombic $Pnma$ phase above 9.5 GPa. The observation of a Fe^{3+} off-center position up to 18 GPa in an average $Pnma$ structure implies that the Fe-cation displacements take place only on a local level, likely in a disordered fashion so that the average structure remains nonpolar. Our observations do not allow discussing the static or dynamic character of such displacements inside the FeO_6 octahedron. We note that a local polar disorder is also observed for some ferroelectrics in an average nonpolar cubic structure at high temperature[59] or at high pressure.[60]

The close relation between oscillator strength and noncentrosymmetric distortions of FeO_6 is well illustrated in Fig. 9. Here $f_{d-d}(^4T_1)$ was derived from the absorption spectra using Eq. (1) and is compared for different Fe^{3+} oxides having different local FeO_6 distortions and distinct Fe-O-Fe exchange pathways. It must be noted that some discrepancies between f_{d-d} values given in Fig. 9 and elsewhere[46,61] are due to the average factor 1/3 used in Eq. (1). Anyway, all f_{d-d} values collected in Fig. 9 are obtained in the same manner through Eq. (1) to allow comparison among different Fe^{3+} oxides.

As it is well known,[41,58] the oscillator strength of crystal-field transition in octahedral $3d^5$ (Mn^{2+}, Fe^{3+}) ions, which are initially spin and parity forbidden by the electric-dipole mechanism in centrosymmetric systems, can be activated by different mechanisms. In order of increasing relevance these

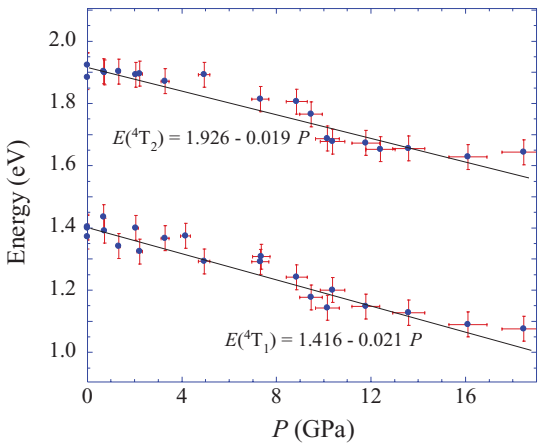

FIG. 8. (Color online) Variation of the $^4T_1$ and $^4T_2$ energies of Fe^{3+} in $BiFeO_3$ with pressure. The straight lines are least-square fits to the pressure dependence $E(P)$. The corresponding linear equations are given inside the figure.

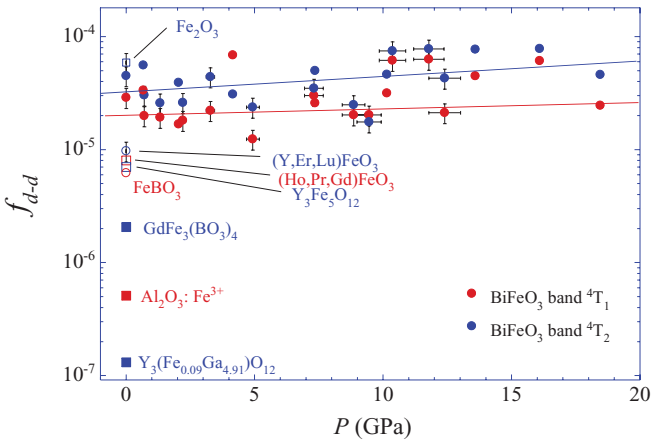

FIG. 9. (Color online) Variation of the transition oscillator strength f_{d-d} of the $^4T_1$ (red/lower) and $^4T_2$ (blue/upper) bands of Fe^{3+} in $BiFeO_3$. The oscillator strength was derived from the integrated band intensity of the two Fe^{3+} bands by fitting from the absorption spectra (see text for explanation). The slight increase of f_{d-d} with pressure unravels an off-center site for Fe^{3+} in the explored pressure range. The ambient pressure points represent the $^4T_1$ oscillator strength obtained from the absorption spectra of different Fe^{3+} oxides: $Y_3Ga_5O_{12}$: Fe^{3+} (Ref. 46); Al_2O_3: Fe^{3+} (Ref. 54); $GdFe_3(BO_3)_4$ (Ref. 51); $FeBO_3$ (Ref. 51); $Y_3Fe_5O_{12}$ (Ref. 46); $(R)FeO_3$ (R: Ho, Pr, Gd; Y, Er, Lu) (Refs. 42 and 44); $BiFeO_3$ present work; and Fe_2O_3 (Ref. 54). Reference numbers refer to absorption and structural data source for obtaining f_{d-d} through Eq. (1).

are noncentrosymmetric distortions of the crystal field induced either dynamically by odd parity vibrations or statically by crystal anisotropy, by the effective spin mechanism in exchange couple pairs, or by exchange interactions and noncentrosymmetric distortions at once.[41,58] Examples of this behavior are found in $Y_3Ga_5O_{12}$: Fe^{3+} (Ref. 46); Al_2O_3: Fe^{3+} (Ref. 54); $GdFe_3(BO_3)_4$ (Ref. 51); $Y_3Fe_5O_{12}$ (Ref. 46); $FeBO_3$ (Ref. 51); $(R)FeO_3$ (R: Ho, Pr, Gd; Y, Er, Lu) (Refs. 42 and 44); and $BiFeO_3$ and Fe_2O_3 (Ref. 54) in order of increasing oscillator strength. At this point we must note that the $^4T_1$ oscillator strength in Fe_2O_3 and $BiFeO_3$ ($f_{d-d} \approx 3$–5×10^{-5}) is about four times larger than the corresponding one in orthoferrites $(R)FeO_3$ and $FeBO_3$, where Fe^{3+} coordination corresponds to a regular FeO_6 octahedron at variance with the off-center displacement attained in the former compounds. Besides activation by the exchange mechanism, an additional contribution to the oscillator strength arises from noncentrosymmetric Fe^{3+} distortions in Fe_2O_3 and $BiFeO_3$, in agreement with results given elsewhere.[41] Accordingly, a hypothetical change of local structure in $BiFeO_3$ yielding a nearly centrosymmetric site around Fe^{3+} (on-center position) would decrease f_{d-d} by at least a factor four due to partial cancellation of the nonparity mechanism.[41] On this basis the results of Fig. 9 suggest that the electric dipole associated with off-center position of Fe^{3+} within FeO_6 still persists at high pressure (18 GPa), although we are not able to extract structural information on the off-center Fe^{3+} displacements from absorption measurements. These findings are similar to those obtained in Fe_2O_3 hematite. Structural studies from XRD under high pressure conditions show that the α-Fe_2O_3 phase with off-center Fe^{3+} is stable up to 30 GPa.[62]

V. CONCLUSIONS

We have demonstrated that crystal-field spectroscopy in Fe^{3+} oxides (hematite, goethite, orthoferrites, etc.) is a useful probe to explore noncentrosymmetric local distortions of the FeO_6 octahedron through the Fe^{3+} transition oscillator strength. f_{d-d} substantially reduces (about a factor four) on passing from off-center Fe^{3+} sites to centrosymmetric Fe^{3+} sites. Optical absorption measurements under pressure in $BiFeO_3$ reveal that the off-center position of Fe^{3+} in the ferroelectric $R3c$ phase remains stable in the nonpolar $Pnma$ phase up to 18 GPa, similar to observations by XRD in Fe_2O_3. Moreover, we have shown that pressure induces linear redshift of both $^4T_1$ and $^4T_2$ bands, which are consistent with a FeO_6 compression concomitant with the crystal compression; i.e., the relative variation of R_{Fe-O} and the pseudocubic lattice parameter is similar. The slight increase of the $^4T_1$ (and $^4T_2$) oscillator strength ($f_{d-d} \approx 3 \times 10^{-5}$) with pressure and the absence of anomalies in $f_{d-d}(P)$ on passing from the rhombohedral $R3c$ phase to the orthorhombic $Pnma$ phase unravels that Fe^{3+} off-center displacements in FeO_6 still persist in the high-pressure phase up to 18 GPa. Despite the weak sensitivity of Fe^{3+} d-d transitions to structural phase transitions in $BiFeO_3$, the band-gap energy $E_{gap}(P)$ and the Raman frequencies $\nu(P)$ do both exhibit noticeable anomalies at the phase-transition pressure, making them suitable probes to detect and characterize different pressure-induced crystal phases in $BiFeO_3$. In summary, we conclude that the structural phase transition at high pressure has a mixed character: displacive (seen through soft modes) and order-disorder (local displacements from absorption). This is a common case in ferroelectric materials, such as $BaTiO_3$, and in this situation it is equally common to observe different characters by different techniques, essentially depending on the correlation length.

ACKNOWLEDGMENTS

Financial support from the Spanish Ministerio de Educación y Ciencia (Project No MAT2008-06873-C02-01), and MALTA CONSOLIDER-INGENIO 2010 (Ref. CDS2007-0045) is acknowledged.

*fernando.rodriguez@unican.es

[1] G. A. Samara, T. Sakudo, and K. Yoshimitsu, Phys. Rev. Lett. **35**, 1767 (1975).
[2] G. A. Samara, J. Phys.: Condens. Matter **15**, 367 (2003).
[3] G. A. Samara, Phys. Rev. Lett. **77**, 314 (1996).
[4] J. Kreisel, B. Noheda, and B. Dkhil, Phase Transitions **82**, 633 (2009).
[5] I. A. Kornev, L. Bellaiche, P. Bouvier, P. E. Janolin, B. Dkhil, and J. Kreisel, Phys. Rev. Lett. **95**, 196804 (2005).
[6] P. E. Janolin, P. Bouvier, J. Kreisel, P. A. Thomas, I. A. Kornev, L. Bellaiche, W. Crichton, M. Hanfland, and B. Dkhil, Phys. Rev. Lett. **101**, 237601 (2008).
[7] Z. Wu and R. E. Cohen, Phys. Rev. Lett. **95**, 037601 (2005).
[8] M. Ahart, M. Somayazulu, P. Dera, H.-K. Mao, R. E. Cohen, R. J. Hemley, R. Yang, and Z. Wu, Nature **451**, 545 (2008).
[9] M. Guennou, P. Bouvier, B. Krikler, J. Kreisel, R. Haumont, and G. Garbarino, Phys. Rev. B **82**, 134101 (2010).
[10] M. Guennou, P. Bouvier, J. Kreisel, and D. Machon, Phys. Rev. B **81**, 054115 (2010).
[11] P. Bouvier and J. Kreisel, J. Phys.: Condens. Matter **14**, 3981 (2002).
[12] J. Zhao, N. L. Ross, and R. J. Angel, J. Phys.: Condens. Matter **16**, 8763 (2004).
[13] R. J. Angel, J. Zhao, and N. L. Ross, Phys. Rev. Lett. **95**, 025503 (2005).
[14] R. H. Mitchell, *Perovskites: Modern and Ancient* (Almaz Press, Inc., Ontario, 2002).
[15] A. M. Glazer, Acta Crystallogr. Sect. B **28**, 3384 (1972).
[16] A. M. Glazer, Acta Crystallogr. Sect. A **31**, 756 (1975).
[17] I. A. Kornev and L. Bellaiche, Phase Transitions **80**, 385 (2007).
[18] A. I. Frenkel, F. M. Wang, S. Kelly, R. Ingalls, D. Haskel, E. A. Stern, and Y. Yacoby, Phys. Rev. B **56**, 10869 (1997).
[19] R. Comès, M. Lambert, and A. Guinier, Solid State Commun. **6**, 715 (1970).
[20] S. Ravy, J.-P. Itié, A. Polian, and M. Hanfland, Phys. Rev. Lett. **99**, 117601 (2007).
[21] Y. Yacoby and Y. Girshberg, Phys. Rev. B **77**, 064116 (2008).
[22] Y. Girshberg and Y. Yacoby, J. Phys. Condens. Matter **24**, 015901 (2012).

[23]G. Catalan and J. F. Scott, Adv. Mater. **21**, 2463 (2009).
[24]R. Haumont, J. Kreisel, and P. Bouvier, Phase Transitions **79**, 1043 (2006).
[25]R. Haumont, P. Bouvier, A. Pashkin, K. Rabia, S. Frank, B. Dkhil, W. A. Crichton, C. A. Kuntscher, and J. Kreisel, Phys. Rev. B **79**, 184110 (2009).
[26]M. Guennou, P. Bouvier, R. Haumont, G. Garbarino, and J. Kreisel, Phase Transitions **84**, 474 (2011).
[27]A. G. Gavriliuk, I. S. Lyubutin, and V. V. Struzhkin, JETP Lett. **86**, 532 (2007).
[28]A. G. Gavriliuk, V. V. Struzhkin, I. S. Lyubutin, I. A. Trojan, M. Y. Hu, and P. Chow, Mater. Res. Soc. Symp. Proc. **987**, PP05 (2007).
[29]A. G. Gavriliuk, V. V. Struzhkin, I. S. Lyubutin, M. Y. Hu, and H. K. Mao, J. Exp. Theor. Phys. Lett. **82**, 224 (2005).
[30]A. G. Gavriliuk, V. V. Struzhkin, I. S. Lyubutin, S. G. Ovchinnikov, M. Y. Hu, and P. Chow, Phys. Rev. B **77**, 155112 (2008).
[31]A. A. Belik, H. Yusa, N. Hirao, Y. Ohishi, and E. Takayama-Muromachi, Chem. Mater. **21**, 3400 (2009).
[32]Y. Yang, L. G. Bai, K. Zhu, Y. L. Liu, S. Jiang, J. Liu, J. Chen, and X. R. Xing, J. Phys.: Condens. Matter **21**, 385901 (2009).
[33]J. L. Zhu, S. M. Feng, L. J. Wang, C. Q. Jin, X. H. Wang, L. T. Li, Y. C. Li, X. D. Li, and J. Liu, High Press. Res. **30**, 265 (2010).
[34]M. Guennou, P. Bouvier, G. S. Chen, B. Dkhil, R. Haumont, G. Garbarino, and J. Kreisel, Phys. Rev. B **84**, 174107 (2011).
[35]D. P. Kozlenko, A. A. Belik, A. V. Belushkin, E. V. Lukin, W. G. Marshall, B. N. Savenko, and E. Takayama-Muromachi, Phys. Rev. B **84**, 094108 (2011).
[36]R. Haumont, R. Saint-Martin, and C. Byl, Phase Transitions **81**, 881 (2008).
[37]B. A. Moral and F. Rodríguez, Rev. Sci. Instrum. **66**, 5178 (1995).
[38]F. Aguado, Ph.D. dissertation, University of Cantabria, 2005.
[39]A. B. P. Lever, *Inorganic Electronic Spectroscopy: Studies in Physical and Theoretical Chemistry* (Elsevier, New York, 1984).
[40]M. N. Sanz-Ortiz, F. Rodríguez, I. Hernández, R. Valiente, and S. Kück, Phys. Rev. B **81**, 045114 (2010).
[41]R. G. Burns, *Mineralogical Applications of Crystal Field Theory* (Cambridge University Press, Cambridge, 1993).
[42]D. L. Wood, J. P. Remeika, and E. D. Kolb, J. Appl. Phys. **41**, 5315 (1970).
[43]Y. Yang, L. G. Bai, K. Zhu, Y. L. Liu, S. Jiang, J. Liu, J. Chen, and X. R. Xing, J. Phys.: Condens. Matter **21**, 385901 (2009).
[44]I. S. Lyubutin and A. G. Gavriliuk, Phys. Usp. **52**, 989 (2009).
[45]B. Ramachandran, A. Dixit, R. Naik, G. Lawes, and M. S. Ramachandra Rao, Phys. Rev. B **82**, 012102 (2010).
[46]G. B. Scott, D. E. Lacklison, and J. L. Page, Phys. Rev. B **10**, 971 (1975).
[47]J. Hlinka, J. Pokorny, S. Karimi, and I. M. Reaney, Phys. Rev. B **83**, 020101 (2011).
[48]P. Hermet, M. Goffinet, J. Kreisel, and Ph. Ghosez, Phys. Rev. B **75**, 220102(R) (2007).
[49]R. P. S. M. Lobo, R. L. Moreira, D. Lebeugle, and D. Colson, Phys. Rev. B **76**, 172105 (2007).
[50]P. Rovillain, M. Cazayous, Y. Gallais, A. Sacuto, R. P. S. M. Lobo, D. Lebeugle, and D. Colson, Phys. Rev. B **79**, 180411 (2009).
[51]A. M. Kalashnikova, V. V. Pavlov, R. V. Pisarev, L. N. Bezmaternykh, M. Bayer, and Th. Rasing, JETP Lett. **80**, 293 (2004).
[52]A. Smakula, Z. Phys. **59**, 603 (1930).
[53]A. Kumar, R. C. Rai, N. J. Podraza, S. Denev, M. Ramirez, Y. H. Chu, L. W. Martin, J. Ihlefeld, T. Heeg, J. Schubert, D. G. Schlom, J. Orenstein, R. Ramesh, R. W. Collins, J. L. Musfeldt, and V. Gopalan, Appl. Phys. Lett. **92**, 121915 (2008).
[54]G. Lehmann and H. Harder, Am. Mineral. **55**, 98 (1970).
[55]H. G. Drickamer and C. W. Frank, *Electronic Transitions and the High Pressure Chemistry and Physics of Solids* (Chapman and Hall, London, 1973).
[56]F. Rodríguez, D. Hernández, and H. U. Güdel, Phys. Rev. B **60**, 10598 (1999).
[57]S. Sugano, Y. Tanabe, and H. Kamimura, *Multiplets of Transition-Metal Ions* (Academic Press, New York, 1970).
[58]Y. Rodríguez-Lazcano, L. Nataf, and F. Rodríguez, Phys. Rev. B **80**, 085115 (2009).
[59]H. Uwe, K. B. Lyons, H. L. Carter, and P. A. Fleury, Phys. Rev. B **33**, 6436 (1986).
[60]J. P. Itié, B. Couzinet, A. Polian, A. M. Flanck, and P. Lagarde, Europhys. Lett. **74**, 706 (2006).
[61]X. S. Xu, T. V. Brinzari, S. Lee, Y. H. Chu, L. W. Martin, A. Kumar, S. McGill, R. C. Rai, R. Ramesh, V. Gopalan, S. W. Cheong, and J. L. Musfeldt, Phys. Rev. B **79**, 134425 (2009).
[62]S. Ono, T. Kikegawa, and Y. Ohishi, J. Phys. Chem. Solids **65**, 1527 (2004).